RESEARCH ARTICLE • OPEN ACCESS

Numerical Investigation of Vertical Oscillations of a Buoyant Object in a Stratified Fluid

Fathya Rabiatunisa, Diki Fernandi and Ikha Magdalena

Volume 14, Issue 1, Pages 138–150, April 2026

Received 3 February 2026, Revised 15 April 2026, Accepted 18 April 2026, Published 23 April 2026

To Cite this Article : F. Rabiatunisa, D. Fernandi and I. Magdalena,"Numerical Investigation of Vertical Oscillations of a Buoyant Object in a Stratified Fluid", *Euler J. Ilm. Mat. Sains dan Teknol.*, vol. 14, no. 1, pp. 138–150, 2026, *https://doi.org/10.37905/euler.v14i1.37621*

JOURNAL INFO • EULER : JURNAL ILMIAH MATEMATIKA, SAINS DAN TEKNOLOGI

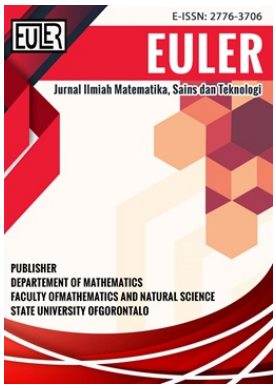

Homepage	:	http://ejurnal.ung.ac.id/index.php/euler/index
Journal Abbreviation	:	Euler J. Ilm. Mat. Sains dan Teknol.
Frequency	:	Three times a year
Publication Language	:	English (preferable), Indonesia
DOI	:	https://doi.org/10.37905/euler
Online ISSN	:	2776-3706
License	:	Creative Commons Attribution-NonCommercial 4.0 International License
Publisher	:	Department of Mathematics, Universitas Negeri Gorontalo
Country	:	Indonesia
OAI Address	:	http://ejurnal.ung.ac.id/index.php/euler/oai
Google Scholar ID	:	QF_r-_gAAAAJ
Email	:	euler@ung.ac.id

JAMBURA JOURNAL • FIND OUR OTHER JOURNALS

Jambura Journal of Biomathematics

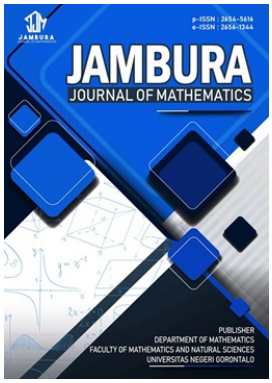

Jambura Journal of Mathematics

Jambura Journal of Mathematics Education

Jambura Journal of Probability and Statistics

Euler : Jurnal Ilmiah Matematika, Sains dan Teknologi, Volume 14, Issue 1, Pages 138–150, April 2026 *https://doi.org/10.37905/euler.v14i1.37621*

Research Article

Check for updates

Numerical Investigation of Vertical Oscillations of a Buoyant Object in a Stratified Fluid

Fathya Rabiatunisa[1], **Diki Fernandi**[1], **Ikha Magdalena**[1,2,*]

[1]*Department of Mathematics, Institut Teknologi Bandung, Bandung 40132, Indonesia*
[2]*Center for Marine and Coastal Development, Institut Teknologi Bandung, Bandung 40132, Indonesia*

ARTICLE HISTORY
Received 3 February 2026
Revised 15 April 2026
Accepted 18 April 2026
Published 23 April 2026

KEYWORDS
Vertical Oscillations
Buoyant Object
Finite Difference Method
Brunt–Väisälä Frequency

ABSTRACT. *This study explores the vertical oscillation dynamics of a buoyant object in a linearly stratified fluid and assesses the accuracy of a first-order finite difference scheme used for numerical simulation. The mathematical formulation, derived from the harmonic motion equation, was solved analytically through linearization around the equilibrium position and numerically to evaluate the scheme's stability and precision. A sensitivity analysis with respect to the time step (Δt) revealed that numerical accuracy strongly depends on temporal resolution: at $\Delta t = 1$ s, the numerical results closely matched the analytical solution, whereas larger Δt values caused noticeable phase errors and reduced precision. As Δt increased, phase errors became noticeable, with discrepancies appearing more clearly at $\Delta t = 5$ s and beyond, highlighting a trade-off between computational efficiency and precision. The model was further extended by incorporating a quadratic damping term (R), enabling the simulation of damped oscillatory motion. Results showed that the decay rate of oscillations increases proportionally with R, where higher friction coefficients ($R = 0.2$) lead to faster energy dissipation and stabilization compared to smaller ones ($R = 0.05$). These outcomes demonstrate the robustness and reliability of the proposed numerical approach in reproducing both undamped and damped oscillation behaviors. This study provides a reliable framework for simulating buoyant object oscillations in stratified fluids, though further development is needed to incorporate more complex hydrodynamic effects for enhanced predictive accuracy.*

1. Introduction

Vertical density stratification, governed by variations in temperature and salinity, creates a dynamically stable fluid environment commonly observed in oceans and lakes. In such environments, buoyant objects exhibit characteristic oscillatory motion when displaced from their equilibrium position [1]. This stratification divides the water column into layers of varying density, which play a fundamental role in ocean mixing, biological transport, and the generation of internal waves [2, 3]. When an object is released within a stratified fluid, it undergoes vertical oscillations driven by a restoring force resulting from the imbalance between gravitational and buoyant forces. This restoring mechanism is strongly influenced by the ambient density gradient, typically characterized by the Brunt–Väisälä frequency [4, 5]. Consequently, the object tends to return toward its equilibrium position, leading to oscillatory motion that reflects the stability properties of the stratified medium [6, 7].

Although the fundamental theory of internal waves and the Brunt–Väisälä frequency is well established [6], accurately predicting the motion of finite-sized objects, as opposed to idealized fluid parcels, remains a challenging problem. This complexity arises from the interplay of several physical mechanisms, including nonlinear buoyancy restoration, added-mass

*Corresponding Author.

Email : *ikha.magdalena@itb.ac.id* (I. Magdalena)
Homepage : http://ejurnal.ung.ac.id/index.php/euler/index / E-ISSN : 2776-3706

effects, and fluid drag. Recent advances in computational techniques, particularly high-fidelity Computational Fluid Dynamics (CFD), have significantly improved the understanding of such phenomena. CFD studies have revealed intricate flow structures accompanying oscillatory motion in stratified fluids [8]. For example, [9] demonstrated that oscillating spheres in stratified fluids can generate complex flow features, including trailing jets and vortex structures, while [10] highlighted the influence of non-Boussinesq effects on oscillation dynamics. Moreover, [11] investigated wake structures and energy dissipation mechanisms, showing notable deviations from behaviors observed in homogeneous fluids.

Experimental studies have also helped validate these numerical findings. Using advanced Particle Image Velocimetry (PIV), [12] analyzed the wake dynamics of oscillating spheres in stratified environments and identified distinct vortex regimes. Similarly, [13] employed synthetic schlieren techniques to measure drag coefficients, confirming enhanced drag near the buoyancy frequency. Comprehensive experiments conducted by [14] further demonstrated that particle shape influences oscillation characteristics, challenging the assumption of universal behavior among buoyant bodies. Despite these advances, both high-fidelity simulations and detailed experiments often involve substantial complexity and cost, making them less suitable for rapid analysis or theoretical interpretation. However, most of these complex hydrodynamic effects are not explicitly considered in reduced-order models, including the present study, which focuses on capturing the primary buoyancy-driven oscillatory dynamics.

The role of added mass in stratified environments has received considerable attention. For instance, [11] showed that added-mass coefficients vary with stratification strength and oscillation frequency, while [15] proposed theoretical formulations accounting for spatial density variations. These findings highlight the limitations of directly applying classical hydrodynamic models originally developed for homogeneous fluids to stratified systems. In addition, nonlinear effects introduce further complexity. Studies have reported nonlinear regime transitions [16], harmonic responses [17], and memory effects in stratified flows [18], indicating that simplified or quasi-steady assumptions may not fully capture the observed dynamics.

Despite these advances, a significant gap remains between high-fidelity simulations and practical predictive models. While CFD approaches [9–11] provide detailed physical insights, their high computational cost limits large-scale parametric exploration and theoretical analysis. In contrast, simplified analytical models often rely on early-stage linearization [19, 20], which may neglect important nonlinear effects, particularly under large-amplitude oscillations. Although nonlinear formulations have been proposed [21, 22], systematic comparisons between fully nonlinear numerical solutions and their linearized analytical counterparts remain limited. Furthermore, realistic nonlinear (quadratic) damping effects, which are essential in oceanographic and environmental contexts [23, 24], are often oversimplified in analytical treatments.

This study presents a reduced-order model that aims to bridge the gap between high-fidelity simulations and simplified analytical approaches by providing both an analytical solution and a validated numerical scheme for stratified oscillatory motion. The system is formulated as a second-order nonlinear ordinary differential equation derived from Newton's second law and Archimedes' principle, incorporating the effects of the ambient density gradient, which is locally approximated as linear in the vicinity of the equilibrium position. To enable analytical insight, the governing equations are linearized about the equilibrium position, yielding a closed-form solution that describes simple harmonic motion while retaining the key physical mechanisms governing the system.

To validate the analytical solution, an explicit finite-difference scheme based on the Forward Euler method is employed. The numerical scheme is verified for first-order consistency and stability through eigenvalue analysis. Simulations are first performed in the absence of damping and compared with the analytical solution for validation. The model is then extended to incorporate frictional effects through quadratic damping, enabling the investigation of more realistic oscillatory dynamics relevant to oceanic and limnological applications, with particular emphasis on the influence of damping on the object's position and velocity responses.

The remainder of this paper is organized as follows. Section 2 presents the mathematical model. Section 3 provides the analytical and numerical results along with a detailed discussion, including cases with and without frictional forces. Finally, Section 4 summarizes the main findings and suggests directions for future research.

2. Model

This section presents the formulation of a mathematical model describing the vertical motion of a buoyant object in a stratified fluid. The model is derived under several simplifying assumptions. The motion is restricted to one-dimensional vertical displacement. The ambient fluid is assumed to be stationary and continuously stratified. Hydrodynamic effects such as added mass, history force, and wake interaction are neglected. In addition, the object is assumed to maintain constant volume, shape, and orientation throughout its motion.

Under these assumptions, the ambient density is modeled as a function of the vertical coordinate according to the Brunt–Väisälä relation:

$$\rho_{amb}(z) = \rho_0 \exp\left(-\frac{N^2}{g} z\right), \tag{1}$$

where $\rho_{amb}(z)$ denotes the ambient density at vertical position z, ρ_0 is the reference density at the surface, N is the Brunt–Väisälä frequency, and g is the gravitational acceleration. The vertical coordinate z is taken positive upward. This stratification implies that the buoyant force depends explicitly on the vertical position through the ambient density profile.

An object of mass M_{obj} and volume V_{obj} located at position z is subjected to two primary forces: gravity acting downward and buoyancy acting upward (see Figure 1).

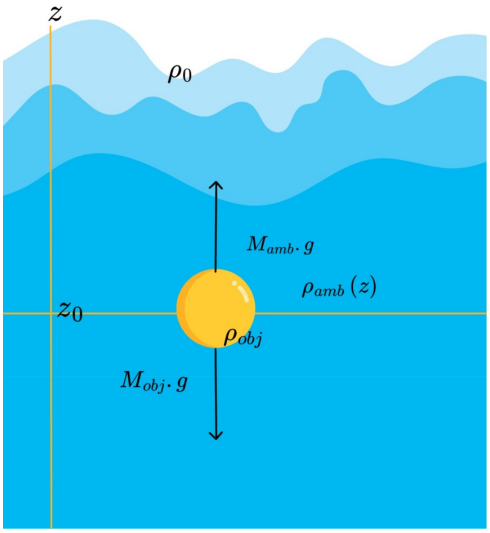

Figure 1. Visualization of a buoyant object and the forces acting upon it

According to Newton's second law, the motion of the object satisfies

$$M_{\text{obj}}\frac{dw}{dt} = F_g + F_b, \tag{2}$$

where $z(t)$ denotes the vertical position and $w = \frac{dz}{dt}$ represents the vertical velocity. The gravitational force is given by

$$F_g = -M_{\text{obj}}g, \tag{3}$$

while the buoyant force is expressed as

$$F_b = \rho_{amb}(z)V_{\text{obj}}g. \tag{4}$$

Substituting these expressions into the force balance yields

$$M_{\text{obj}}\frac{dw}{dt} = -M_{\text{obj}}g + \rho_{amb}(z)V_{\text{obj}}g. \tag{5}$$

By Archimedes' principle, the mass of the displaced fluid is given by

$$M_{amb} = \rho_{amb}(z)V_{\text{obj}}, \tag{6}$$

where M_{amb} denotes the mass of the displaced ambient fluid. The mass of the object is expressed as

$$M_{\text{obj}} = \rho_{\text{obj}}V_{\text{obj}}, \tag{7}$$

where ρ_{obj} denotes the density of the object.

Dividing both sides by M_{obj} and substituting eq. (6) and eq. (7), we obtain the system

$$\begin{cases} w_t = -g\dfrac{\rho_{\text{obj}} - \rho_{amb}(z)}{\rho_{\text{obj}}}, \\ z_t = w, \end{cases} \tag{8}$$

where $w_t = \dfrac{dw}{dt}$ denotes the vertical acceleration and $z_t = \dfrac{dz}{dt}$ denotes the vertical velocity.

The system in eq. (8) can be reduced to a single nonlinear second-order differential equation for the vertical position $z(t)$:

$$z_{tt} + g\frac{\rho_{\text{obj}} - \rho_{amb}(z)}{\rho_{\text{obj}}} = 0. \tag{9}$$

Eq. (9) illustrates the competition between the object density and the depth-dependent ambient density. The dynamics therefore resemble a nonlinear oscillator, in which buoyancy acts as a restoring force governed by the stratification profile.

3. Results and Discussion

This section presents the analytical and numerical results of the study, followed by a detailed discussion to evaluate their accuracy and physical implications. The comparison between the analytical solution and numerical simulations is also provided to assess the performance of the proposed method under different conditions.

3.1. Analytical Solution

We derive the analytical solution of eq. (9) by first identifying the equilibrium position of the object in the stratified fluid. Let $\overline{z}$ denote the equilibrium depth (see Figure 1), defined as the position where the net force acting on the object vanishes. At this point, the gravitational force is exactly balanced by the buoyant force.

Physically, this condition is satisfied when the density of the object equals the ambient fluid density at that depth, i.e.,

$$\rho_{obj} = \rho_{amb}(\overline{z}). \tag{10}$$

Using the Brunt–Väisälä density profile in eq. (1), and assuming small density variations such that the exponential function can be approximated by its first-order Taylor expansion, the equilibrium position can be expressed as

$$\overline{z} = -g\frac{\rho_{obj} - \rho_0}{\rho_0 N^2}. \tag{11}$$

To analyze the dynamics near equilibrium, we introduce a small perturbation around the equilibrium position by defining

$$z(t) = \overline{z} + z^*(t),$$

where $z^*(t)$ represents a small displacement from equilibrium. Substituting this expression into eq. (9), we obtain

$$z^*_{tt} + g\frac{\rho_{obj} - \rho_{amb}(\overline{z} + z^*)}{\rho_{obj}} = 0.$$

To linearize the system, we expand $\rho_{amb}(\overline{z} + z^*)$ using a first-order Taylor expansion around $\overline{z}$:

$$\rho_{amb}(\overline{z} + z^*) \approx \rho_{amb}(\overline{z}) + z^*\frac{d\rho_{amb}}{dz}(\overline{z}).$$

Since $\rho_{amb}(\overline{z}) = \rho_{obj}$ at equilibrium, this simplifies to

$$\rho_{obj} - \rho_{amb}(\overline{z} + z^*) \approx -z^*\frac{d\rho_{amb}}{dz}(\overline{z}).$$

Substituting this approximation into the governing equation yields

$$z^*_{tt} - g\frac{1}{\rho_{obj}}\frac{d\rho_{amb}}{dz}(\overline{z})z^* = 0.$$

Using the Brunt–Väisälä relation,

$$\frac{d\rho_{amb}}{dz} = -\frac{N^2}{g}\rho_{amb},$$

and evaluating at $z = \overline{z}$, we obtain

$$\frac{d\rho_{amb}}{dz}(\overline{z}) = -\frac{N^2}{g}\rho_{obj}.$$

Thus, the governing equation reduces to the linear harmonic oscillator:

$$z^*_{tt} + \frac{\rho_0}{\rho_{obj}}N^2 z^* = 0. \tag{12}$$

Eq. (12) represents a simple harmonic motion with general solution

$$z^*(t) = C_1\cos(rNt) + C_2\sin(rNt),$$

where $r^2 = \dfrac{\rho_0}{\rho_{obj}}$, and C_1 and C_2 are constants determined by initial conditions.

Substituting back into $z(t) = \overline{z} + z^*(t)$, the solution for position and velocity becomes

$$\begin{cases} z(t) = C_1 \cos(rNt) + C_2 \sin(rNt) + \overline{z}, \\ w(t) = -C_1 rN \sin(rNt) + C_2 rN \cos(rNt). \end{cases} \tag{13}$$

Assuming that the object is released from an initial position with zero initial velocity, i.e., $w(0) = 0$, it follows from eq. (13) that $C_2 = 0$. The solution therefore reduces to

$$\begin{cases} z(t) = C_1 \cos(rNt) + \overline{z}, \\ w(t) = -C_1 rN \sin(rNt), \end{cases} \tag{14}$$

where the constant C_1 is determined by the initial displacement of the object from equilibrium, namely

$$C_1 = z(0) - \overline{z}.$$

The resulting analytical solution indicates that the object undergoes simple harmonic oscillation about its equilibrium position $\overline{z}$ with angular frequency $\omega = rN$. This frequency depends on both the stratification strength, represented by the Brunt–Väisälä frequency N, and the density ratio ρ_0/ρ_{obj}.

From the velocity expression, it can be observed that the magnitude of the velocity reaches its maximum when the object passes through the equilibrium position ($z = \overline{z}$), where the displacement is zero. Conversely, the velocity becomes zero at the turning points of the motion, corresponding to the maximum displacement from equilibrium. This behavior is consistent with the fundamental characteristics of simple harmonic motion. This analytical solution is valid under the assumption of small perturbations around the equilibrium position, where nonlinear effects are negligible.

3.2. Numerical Method

This section presents the numerical method employed to solve the system of differential equations formulated earlier. The time domain $t \in [0, T]$ is uniformly discretized using a time step Δt, yielding the partition $0 = t^1, t^2, \ldots, t^{N_t+1} = T$. For notational convenience, we define $w(t^n) = w^n$ and $z(t^n) = z^n$.

To discretize system (8), we employ a semi-implicit Euler scheme. In this approach, the velocity is first updated using the known position at time level n, and the position is subsequently updated using the newly computed velocity. Hence, the scheme is written as:

$$\begin{cases} \dfrac{w^{n+1} - w^n}{\Delta t} = -g \dfrac{\rho_{obj} - \rho_{amb}(z^n)}{\rho_{obj}}, \\ \dfrac{z^{n+1} - z^n}{\Delta t} = w^{n+1}. \end{cases} \tag{15}$$

The model is extended by incorporating a quadratic damping term (R), represented by $-R|w|w$, where w is the vertical velocity and R is the friction coefficient. This damping term accounts for energy dissipation, which is common in oscillatory motion and simulates realistic frictional effects in stratified fluids. Accordingly, the update formulas used in the computation are

$$\begin{cases} w^{n+1} = w^n - g \dfrac{\rho_{obj} - \rho_{amb}(z^n)}{\rho_{obj}} \Delta t, \\ z^{n+1} = z^n + w^{n+1} \Delta t. \end{cases} \tag{16}$$

Thus, at each time step, w^{n+1} is computed first, followed by z^{n+1}. This distinction is important because the present discretization is not the standard explicit Forward Euler scheme for both variables, but a semi-implicit Euler-type update.

3.2.1. Consistency

To assess the consistency of the semi-implicit Euler scheme (15), we examine its local truncation error by substituting the exact solution into the discrete equations. Let

$$f(z) = -g\frac{\rho_{obj} - \rho_{amb}(z)}{\rho_{obj}}, \tag{17}$$

where the continuous system can be written as

$$w_t = f(z), \quad z_t = w).$$

Assume that the exact solutions $w(t)$ and $z(t)$ are sufficiently smooth. Expanding $w^{n+1} = w(t^{n+1})$ and $z^{n+1} = z(t^{n+1})$ about t^n gives

$$\begin{aligned} w^{n+1} &= w^n + w_t^n\Delta t + \tfrac{1}{2}w_{tt}^n\Delta t^2 + \mathcal{O}(\Delta t^3), \\ z^{n+1} &= z^n + z_t^n\Delta t + \tfrac{1}{2}z_{tt}^n\Delta t^2 + \mathcal{O}(\Delta t^3). \end{aligned} \tag{18}$$

For the velocity equation, substituting the exact solution into the discrete form yields

$$\frac{w^{n+1} - w^n}{\Delta t} = w_t^n + \tfrac{1}{2}w_{tt}^n\Delta t + \mathcal{O}(\Delta t^2).$$

Using the continuous equation $w_t^n = f(z^n)$, the local truncation error becomes

$$\tau_w^n = \frac{w^{n+1} - w^n}{\Delta t} - f(z^n) = \tfrac{1}{2}w_{tt}^n\Delta t + \mathcal{O}(\Delta t^2).$$

For the position equation, we have

$$\frac{z^{n+1} - z^n}{\Delta t} = z_t^n + \tfrac{1}{2}z_{tt}^n\Delta t + \mathcal{O}(\Delta t^2).$$

Since $z_t = w$ and $z_{tt} = w_t$, the expansion of w^{n+1} is

$$w^{n+1} = w^n + w_t^n\Delta t + \mathcal{O}(\Delta t^2) = z_t^n + z_{tt}^n\Delta t + \mathcal{O}(\Delta t^2).$$

Hence,

$$\tau_z^n = \frac{z^{n+1} - z^n}{\Delta t} - w^{n+1} = -\tfrac{1}{2}z_{tt}^n\Delta t + \mathcal{O}(\Delta t^2).$$

Therefore, both local truncation errors are of order $\mathcal{O}(\Delta t)$, and the semi-implicit Euler scheme is first-order consistent in time.

3.2.2. Stability

In this section, we analyze the stability of the semi-implicit Euler scheme. To facilitate the analysis we consider a linearized form of system (eq. (16)) around the equilibrium state, leading to the following homogeneous system:

$$\begin{aligned} w^{n+1} &= w^n - r^2N^2z^n\Delta t \\ z^{n+1} &= z^n + w^{n+1}\Delta t. \end{aligned}$$

This system can be expressed in matrix form as

$$\begin{pmatrix} w^{n+1} \\ z^{n+1} \end{pmatrix} = \begin{pmatrix} 1 & -r^2N^2\Delta t \\ \Delta t & -r^2N^2\Delta t^2 + 1 \end{pmatrix} \begin{pmatrix} w^n \\ z^n \end{pmatrix} \tag{19}$$

The eigenvalues ($\lambda_{1,2}$) of the coefficient matrix are given by

$$\lambda_{1,2} = 1 - \frac{r^2N^2\Delta t^2}{2} \pm \frac{\sqrt{(r^2N^2\Delta t^2)^2 - 4r^2N^2\Delta t^2}}{2} \tag{20}$$

The magnitude of the eigenvalues determines the stability behavior of the scheme. For oscillatory systems, the eigenvalues are generally complex, and their modulus depends on the time step Δt. This indicates that the stability of the scheme is not unconditional, but instead depends on the choice of Δt. In particular, for sufficiently small Δt, the numerical solution remains bounded and exhibits stable oscillatory behavior. However, for larger values of Δt, deviations from the analytical solution may occur, as also observed in the numerical experiments. Therefore, the stability of the scheme depends on the choice of the time step size.

3.3. Discussion

Here, a numerical scheme is applied to analyze the vertical motion of a buoyant object assumed to be within a linearly stratified seawater environment. The simulation assumes the fluid density increases from $1025\,\text{kg/m}^3$ at the surface (d_0) to $1026\,\text{kg/m}^3$ at a depth of 100 meters (d_{100}). The stability of this fluid stratification is characterized by the Brunt-Väisälä frequency parameter, whose squared value is $N^2 = 10^{-4}\,\text{s}^{-2}$, which is a fundamental parameter governing oscillatory motion in stratified fluids [1, 6].

The analysis is conducted on an object with a density $1025.5\,\text{kg/m}^3$ that is released at a depth of 80 meters. Since this object's density lies between the surface and bottom water densities, it will have an equilibrium position where its density is equivalent to the density of the surrounding fluid. Based on the linear density model, this equilibrium point is calculated to be at a depth of 50 meters. The unbalanced buoyant force at the 80-meter depth causes the object to undergo a vertical oscillation around this equilibrium point.

When placed at an initial depth of 80 meters, the object will undergo simple harmonic oscillation around its equilibrium position, which is a well-known behavior in stably stratified environments where buoyancy acts as a restoring force [6, 20]. This oscillatory motion can be described analytically by the equation:

$$z(t) = (-30)\cos(rNt) + 50 \tag{21}$$

To verify the analytical solution and to explore the model's behavior numerically, simulations are conducted both with and without frictional forces.

3.3.1. Without Frictional Forces

In the initial simulation, we investigate the vertical motion of a buoyant object while neglecting the effect of friction forces. The object is released from an initial depth of $d_0 = 80$ meters. As presented in Figure 2, the simulation results compare the analytical and numerical solutions, focusing on the object's position and velocity.

The results summarized in Table 1 clearly show that the accuracy of the numerical scheme strongly depends on the time step (Δt). For $\Delta t = 1$ s (see Figure 2a), the numerical solution for both position (z) and velocity (w) closely matches the analytical solution. This is supported

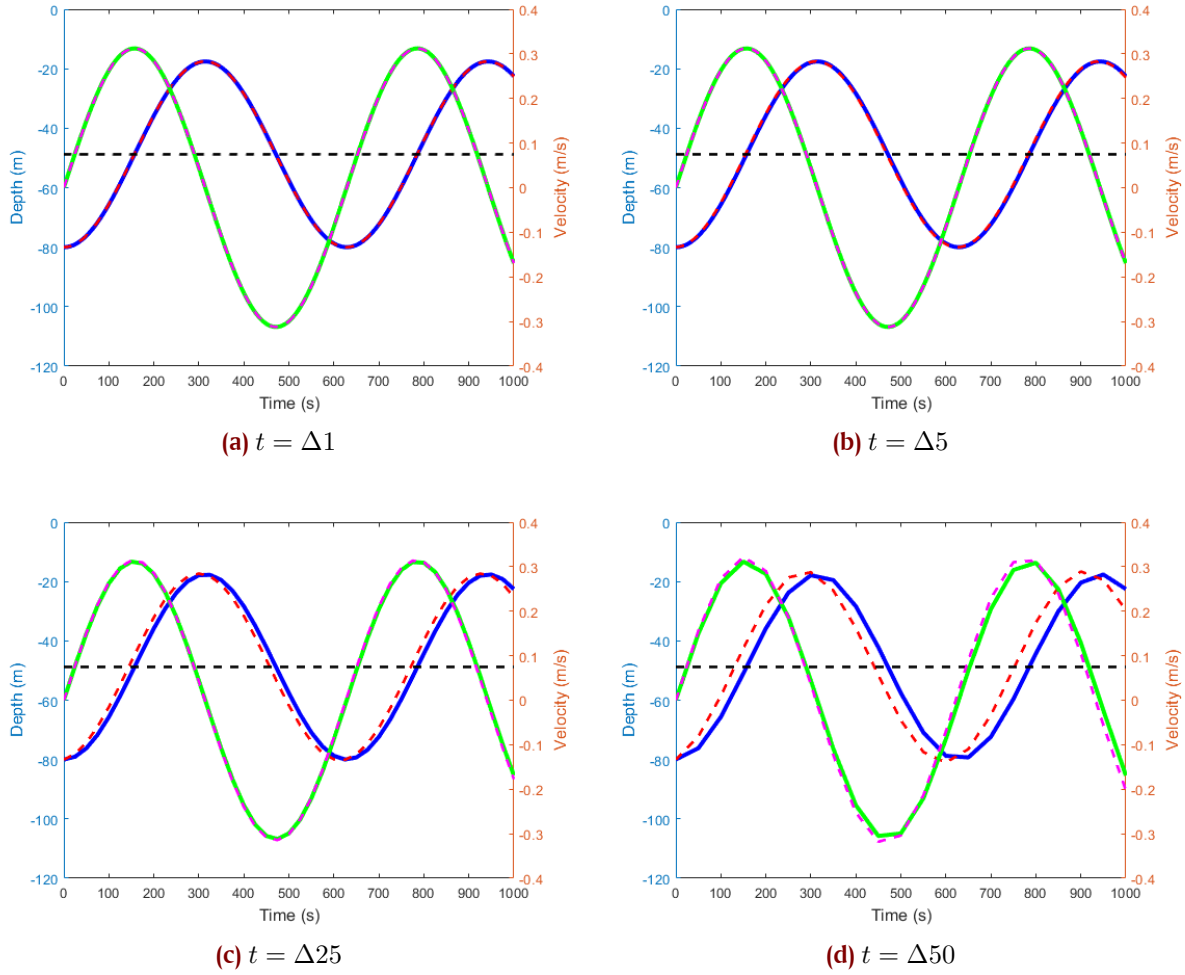

(a) $t = \Delta 1$ **(b)** $t = \Delta 5$

(c) $t = \Delta 25$ **(d)** $t = \Delta 50$

Figure 2. Comparison of analytical solution (dashed line) and numerical solution (solid line) for object's position (blue and red lines) and its velocity (green and purple lines) based on Δt

Table 1. Error metrics for different time step sizes

Δt	RMSE	L_2 Norm	Amp. Error	Phase Error (s)	MAE	MRE	Avg. Time (s)
1	0.108	3.423	0.000	0.00	0.096	0.002	0.00118
5	0.548	17.410	0.010	5.00	0.487	0.010	0.00103
25	2.970	95.040	0.200	25.00	2.640	0.070	0.00099
50	6.640	215.000	1.010	50.00	5.880	0.150	0.00036

by the very small error values (RMSE = 0.108, MAE = 0.096, and negligible amplitude and phase errors), indicating high accuracy and consistency at fine temporal resolution.

When the time step is increased to $\Delta t = 5$ s (see Figure 2b), small discrepancies begin to appear. This is reflected in the increase of RMSE to 0.548 and the emergence of a phase error of 5 s, although the overall agreement between numerical and analytical solutions remains acceptable. For $\Delta t = 25$ s (see Figure 2c), the deviation becomes more pronounced. The error metrics increase significantly (RMSE = 2.970, MAE = 2.640), accompanied by a larger amplitude error (0.200) and phase error of 25 s, indicating that the numerical solution begins to lose accuracy in capturing both magnitude and timing of the oscillation.

At the largest time step, $\Delta t = 50$ s (see Figure 2d), the numerical error becomes substantial. The RMSE rises to 6.640 and MAE to 5.880, while the amplitude error exceeds 1.0. Notably, the phase error reaches 50 s, indicating a significant temporal shift between the

numerical and analytical solutions. This confirms that the numerical scheme fails to accurately resolve the oscillatory behavior at coarse time resolution. These results highlight a fundamental trade-off in the numerical approach: although increasing the time step reduces computational time (as shown by the decreasing average computation time in Table 1), it significantly degrades solution accuracy. This behavior is typical in numerical simulations of oscillatory and stratified systems [8, 21].

Physically, the phase relationship between depth and velocity remains consistent with harmonic motion. The velocity reaches its maximum magnitude when the object passes through the equilibrium position and becomes zero at extreme displacements, in agreement with classical descriptions of oscillatory motion in stratified fluids [6].

The physical movement of the object during oscillation is also reinforced through the visual representation shown in Figure 2. The object appears to move away from and then return to the equilibrium point, which confirms the oscillation pattern predicted by the analytical model. This motion is driven by the net buoyant force that acts as a restoring force, pulling the object back to the position where its density is proportional to the density of the surrounding fluid.

3.3.2. With Frictional Forces

Next, scheme (16) is modified by adding a friction force represented by the deceleration term $-R|w|w$. This damping term is discretized to obtain a finite difference scheme for updating the velocity and position of the object. The resulting scheme can be written as

$$\begin{aligned} w^{n+1} &= \frac{w^n - g\dfrac{\rho_{\text{obj}} - \rho_{\text{amb}}(z^n)}{\rho_{\text{obj}}}\Delta t}{1 + R|w^n|\Delta t}, \\ z^{n+1} &= z^n + w^{n+1}\Delta t. \end{aligned} \tag{22}$$

Eq. (22) accounts for the effect of gravity, the density difference between the object and the surrounding fluid, as well as the damping contribution from the friction coefficient R. In the simulations, two values of the friction coefficient are considered, namely $R = 0.05$ and $R = 0.2$, in order to compare the influence of friction on the dynamics of the object's velocity and position.

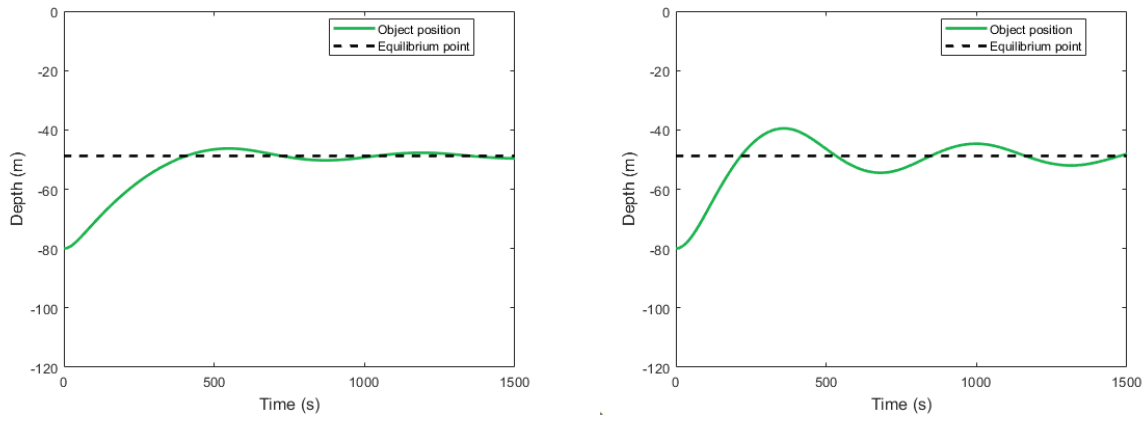

(a) $R = 0.2$ **(b)** $R = 0.05$

Figure 3. Comparison of numerical solutions with different friction coefficients R

Figure 3 shows the influence of the friction coefficient R on the vertical motion of the object in a linearly stratified fluid. The presence of friction introduces a resistive force that opposes the motion, effectively reducing the object's acceleration during both ascent and descent. As a result, the amplitude of oscillation around the equilibrium position no longer remains constant but gradually diminishes over time due to the continuous loss of kinetic energy. Initially, the object, being denser than the surrounding fluid at its starting depth, experiences a buoyant acceleration upwards. However, as it moves through layers of increasing density, the buoyant force decreases, leading to oscillatory motion about the equilibrium depth. The inclusion of friction transforms this motion into a damped oscillation, where the amplitudes of displacement and velocity decay progressively over time, a behavior widely reported in studies of particles and bodies moving in stratified fluids [4, 5]. The trajectory asymptotically approaches the equilibrium point, while the velocity tends toward zero, indicating that the object eventually comes to rest after a sufficiently long period. The damping rate is strongly dependent on the magnitude of the friction coefficient, where larger values of R lead to faster energy dissipation, which is consistent with previous observations on drag-induced damping in stratified environments [12, 13]. For the larger value $R = 0.2$, the oscillations decay rapidly, and the object reaches its equilibrium depth in a relatively short time. In contrast, for the smaller coefficient $R = 0.05$, the system exhibits slower energy dissipation, resulting in a more prolonged oscillatory response before stabilization occurs. This clearly demonstrates that the friction coefficient governs not only the rate of decay of oscillations but also the temporal scale over which dynamic equilibrium is achieved.

4. Conclusion

In this study, an explicit finite difference scheme has been successfully applied to simulate the oscillatory dynamics of a buoyant object in a stratified fluid, under both ideal and damped conditions. The results demonstrate that the numerical accuracy of the scheme is highly sensitive to the chosen time step (Δt). At a fine temporal resolution ($\Delta t = 1$ s), the numerical solution exhibits excellent agreement with the analytical solution, confirming the capability of the scheme to precisely represent harmonic motion. However, as Δt increases, the accuracy declines due to phase shifts and numerical dispersion, highlighting a fundamental trade-off between computational efficiency and precision. The computational model was subsequently enhanced by incorporating a frictional damping term, resulting in realistic damped oscillatory behavior. Simulations using various friction coefficients (R) revealed that the oscillation decay rate is directly proportional to R. Higher R values ($R = 0.2$) induce faster energy dissipation and earlier stabilization, whereas smaller values ($R = 0.05$) yield slower energy attenuation and prolonged oscillation. These findings verify the robustness of the developed numerical approach in capturing both undamped and damped oscillation phenomena. The validated model provides a reliable foundation for future studies aimed at predicting vertical motion and equilibrium positioning of buoyant bodies in layered environments. Further refinement should include vertical hydrodynamic effects such as pressure gradients, stratification-induced flow interaction, and weak nonlinearities to enhance the physical realism and predictive capability of the model.

Author Contributions. **Fathya Rabiatunisa**: Conceptualization, methodology, formal analysis, software, writing original draft preparation. **Diki Fernandi**: Conceptualization, methodology, Software, validation, data curation, visualization, writing review and editing. **Ikha Magdalena**: Conceptualization, methodology, Software, validation, data curation, visualization, writing review and editing.

Acknowledgment. The authors would like to thank the editors and reviewers for their valuable comments and suggestions, which have helped to improve the quality of this manuscript.

Funding. This research received no external funding.

Conflict of interest. The authors declare that they have no known competing financial interests or personal relationships that could have appeared to influence the work reported in this paper.

Data availability. This study is theoretical in nature and does not involve the use of any experimental or observational data. Therefore, data sharing is not applicable.

References

[1] J. Riley and E. Lindborg, "Recent progress in stratified turbulence," *Ten Chapters in Turbulence*, pp. 269–317, Jan. 2010, doi: 10.1017/CBO9781139032810.008.

[2] V. Boatwright and B. Fox-Kemper, "Biological and physical interactions at local ocean scales: Coupled systems," *Georgetown Scientific Research Journal*, pp. 5–17, Feb. 2021, doi: 10.48091/DNPR7287.

[3] S. Legg, "Mixing by oceanic lee waves," *Annual Review of Fluid Mechanics*, vol. 53, 2021, doi: 10.1146/annurev-fluid-051220-043904.

[4] L. Huguet, V. Barge-Zwick, and M. Le Bars, "Dynamics of a reactive spherical particle falling in a linearly stratified fluid," *Physical Review Fluids*, vol. 5, no. 11, p. 114803, 2020, doi: 10.1103/PhysRevFluids.5.114803.

[5] A. Doostmohammadi, S. Dabiri, and A. Ardekani, "A numerical study of the dynamics of a particle settling at moderate reynolds numbers in a linearly stratified fluid," *Journal of Fluid Mechanics*, vol. 750, pp. 5–32, 2014, doi: 10.1017/jfm.2014.243.

[6] A. E. Gill, *Atmosphere–Ocean Dynamics*. Academic Press, 1982, [Online]. Available: https://doi.org/api.semanticscholar.org/CorpusID:116672531.

[7] Y. V. Prikhod'ko and Y. D. Chashechkin, "Hydrodynamics of natural oscillations of neutrally buoyant bodies in a layer of continuously stratified fluid," *Fluid Dynamics*, vol. 41, pp. 545–554, 2006, doi: 10.1007/s10697-006-0072-5.

[8] F. Cocetta, M. Gillard, J. Szmelter, and P. K. Smolarkiewicz, "Stratified flow past a sphere at moderate reynolds numbers," *Computers & Fluids*, vol. 226, p. 104998, 2021, doi: 10.1016/j.compfluid.2021.104998.

[9] H. Hanazaki, K. Kashimoto, and T. Okamura, "Jets generated by a sphere moving vertically in a stratified fluid," *Journal of Fluid Mechanics*, vol. 638, pp. 173–197, 2009, doi: 10.1017/S0022112009990498.

[10] E. Heifetz and J. Mak, "Stratified shear flow instabilities in the non-boussinesq regime," *Physics of Fluids*, vol. 27, no. 8, p. 086601, 2015, doi: 10.1063/1.4928738.

[11] B. Voisin, "Added mass of oscillating bodies in stratified fluids," *Journal of Fluid Mechanics*, vol. 987, p. A27, 2024, doi: 10.1017/jfm.2024.326.

[12] K. Y. Yick, C. R. Torres, T. Peacock, and R. Stocker, "Enhanced drag of a sphere settling in a stratified fluid at small reynolds numbers," *Journal of Fluid Mechanics*, vol. 632, pp. 49–68, 2009, doi: 10.1017/S0022112009007332.

[13] J. Pan, C. Tu, M. Kan, J. Shan, F. Bao, and J. Lin, "Settling velocity variation induced by a sphere moving across a two-layer stratified fluid with different rheological characteristics," *RSC Advances*, vol. 13, pp. 9773–9780, 2023, doi: 10.1039/D3RA00164J.

[14] L. Unglehrt and M. Manhart, "Assessment of models for nonlinear oscillatory flow through a hexagonal sphere pack," *Transport in Porous Media*, vol. 151, pp. 1–31, 2024, doi: 10.1007/s11242-024-02110-y.

[15] I. V. Sturova, "Hydrodynamic loads acting on an oscillating cylinder submerged in a stratified fluid with ice cover," *Journal of Applied Mechanics and Technical Physics*, vol. 52, pp. 415–426, 2011, doi: 10.1134/S0021894411030126.

[16] V. M. Chernyavskii, "Nonlinear instability of the stratified fluid layer of finite thickness," *Doklady Akademii Nauk*, vol. 1, 2005, doi: 10.1134/1.1941494.

[17] J. Yalim, B. D. Welfert, and J. M. Lopez, "Superharmonic and triadic resonances in a horizontally oscillated stably stratified square cavity," *Journal of Fluid Mechanics*, vol. 970, p. A25, 2023, doi: 10.1017/jfm.2023.618.

[18] P. Meunier and G. Spedding, "A loss of memory in stratified wakes," *Physics of Fluids*, vol. 16, pp. 298–305, 2004, doi: 10.1063/1.1630053.

[19] A. Abdeldayem, T. Bon, R. B. Cal, and J. Meyers, "Linear model for secondary motions in stratified flows," *Physical Review Fluids*, vol. 10, no. 1, p. 014605, 2025, doi: 10.1103/PhysRevFluids.10.014605.

[20] M. Carpineti, F. Croccolo, and A. Vailati, "Levitation, oscillations, and wave propagation in a stratified fluid," *European Journal of Physics*, vol. 42, no. 5, p. 055011, 2021, doi: 10.1088/1361-6404/ac0fba.

[21] Y. Jin, K. Xie, G. Liu, Y. Peng, and B. Wan, "Nonlinear dynamics modeling and analysis of a marine buoy single-point mooring system," *Ocean Engineering*, vol. 262, p. 112031, 2022, doi: 10.1016/j.oceaneng.2022.112031.

[22] A. Shafiq, T. N. Sindhu, M. A. Iqbal, and T. A. Abushal, "Nonlinear squeezing flow of stratified fluids: A comprehensive study on convective conditions and probable errors," *International Journal of Thermofluids*, vol. 28, p. 101290, 2025, doi: 10.1016/j.ijft.2025.101290.

[23] G. Ma, J. T. Kirby, S.-F. Su, J. Figlus, and F. Shi, "Numerical study of turbulence and wave damping induced by vegetation canopies," *Coastal Engineering*, vol. 80, pp. 68–78, 2013, doi: 10.1016/j.coastaleng.2013.05.007.

[24] S. Zilitinkevich, O. Druzhinin, A. Glazunov, E. Kadantsev, E. Mortikov, I. Repina, and Y. Troitskaya, "Dissipation rate of turbulent kinetic energy in stably stratified sheared flows," *Atmospheric Chemistry and Physics*, vol. 19, no. 4, pp. 2489–2496, 2019, doi: 10.5194/acp-19-2489-2019.